Multiactuators Control for Prototype Panorama Scanning Imaging With Input Saturation

YUTANG WANG, Member, IEEE
DAPENG TIAN, Senior Member, IEEE
Changchun Institute of Optics, Fine Mechanics and Physics, Chinese Academy of Sciences, Changchun, China and University of Chinese Academy of Sciences Beijing, China

RUI XU, Member, IEEE
Changchun Institute of Optics, Fine Mechanics and Physics, Chinese Academy of Sciences, Changchun, China

In this article, we propose an adaptive sliding mode control scheme with a saturation coefficient (ASMC-SC) for panorama scanning imaging with multiple actuators in the presence of input saturation. By introducing a SC into the sliding surface and adaptive parameters, the actuator drive capability is more fully utilized, and undesired accumulations of adaptive parameters are avoided. A stability analysis was performed using the Lyapunov stability arguments. The simulation and experimental results show that the ASMC-SC guarantees imaging efficiency and has a better tracking performance.

Manuscript received April 15, 2021; revised August 16, 2021 and November 4, 2021; released for publication November 15, 2021. Date of publication November 18, 2021; date of current version June 9, 2022.

DOI. No. 10.1109/TAES.2021.3129152

Refereeing of this contribution was handled by K. P. Judd.

This work was supported in part by the Key Research Program of Frontier Sciences, CAS under Grant ZDBS-LY-JSC044 and in part by the National Science Foundation of China under Grant 61673365.

Authors' addresses: Yutang Wand and Dapeng Tian are with the Key Laboratory of Airborne Optical Imaging and Measurement, Changchun Institute of Optics, Fine Mechanics and Physics, Chinese Academy of Sciences, Changchun 130033, China and also with the University of Chinese Academy of Sciences, Beijing 100049, China, E-mail: (ytwang@ciomp.ac.cn; d.tian@ciomp.ac.cn); Rui Xu is with the Key Laboratory of Airborne Optical Imaging and Measurement, Changchun Institute of Optics, Fine Mechanics and Physics, Chinese Academy of Sciences, Changchun 130033, China, E-mail: (xur@ciomp.ac.cn). *(Corresponding author: Dapeng Tian.)*

I. INTRODUCTION

Aerospace or aerial panorama scanning imaging plays a vital role in disaster prevention and rescue, geographical mapping, precision agriculture, and in other fields [1]–[3].

To achieve wider coverage under a limited field of view (FOV) effectively, scanning imaging is employed by continuously rotating the scanning mirror installed inside the scanning imaging system [4]. During an imaging cycle, imaging system controls the scanning mirror to swing uniformly from its initial scanning position while generating periodic imaging trigger signals that control imaging medium to image multiple times in succession, which can be stitched together into a wide FOV image. However, this stitched FOV still does not meet the requirements of panorama imaging, multiple sets of scanning mirrors and corresponding imaging mediums must be introduced to image simultaneously in different angles of view to obtain a large FOV panoramic image.

Panorama scanning imaging system (PSIS) with multiple actuators brings new control difficulties. On one hand, the physical motion range of scanning mirrors is limited by the imaging mode of PSIS, it is necessary to control the actuators maintain high speed reciprocating motion; on the other hand, it is also essential to guarantee high-precision collaborative motion of multiple actuators, so that all images obtained from the same imaging cycle can be seamlessly stitched together into a large FOV image [5]. The reciprocating and collaborative motion require actuators with sufficient drive capability, which is difficult to achieve owing to the limitations of space, weight, and power in aerospace and aerial PSIS. Consequently, frequent actuator input saturation will happen, causing performance deterioration or even system instability and damage of imaging components [6]. The contradiction between the increasing demand for imaging efficiency and the limited actuation ability is becoming increasingly significant. Making better use of the limited drive capability of actuators to achieve efficient and panorama scanning imaging has become an urgent control problem to be solved.

To solve the difficulties, many control methods have been proposed. When the requirement for imaging efficiency is not quite high, appropriate command planning could be made for PSIS to realize reciprocating motion and imaging, with robust controllers to guarantee imaging performance. Gain-compensated sinusoidal scanning control employing a preemphasis technique was then proposed, which prevents input saturation and performance degradation under triangular waves [7]. Furthermore, a periodic trapezoidal wave command was designed for a PSIS, and a disturbance observer was implemented to compensate for friction and other disturbances [8]. The disturbance observer-based control method can evaluate and compensate for the system lumped disturbances, which are generally asymptotically constant or slowly varying disturbances. However, when there are disturbances with high nonlinearity, such as input saturation, the method is no longer valid, and the tracking performance of multiactuators deteriorates.

Consequently, to achieve satisfactory imaging performance, a certain amount of driving margin must be reserved to avoid input saturation, which limits the imaging efficiency of PSIS.

Owing to the development of the control system in aerospace/aerial systems, it is possible for practical applications to introduce auxiliary controller or compensator for suppressing input saturation. The auxiliary systems related to saturation are introduced to compensate for input saturation [9]–[11]. An antiwindup compensator system is designed to simultaneously achieve full-state constraints and input saturation for noncooperative spacecraft fly-around missions [12]. In the context of quadrotor unmanned aerial vehicles (UAVs), two control allocation strategies are presented, with the aim of avoiding output saturation [13]. These methods avoid the control system from entering saturation, but also limit motion rapidity to some extent.

Sliding mode control (SMC) is implemented in all types of control systems owing to its robustness to disturbances and the rapidity of response [14]. A class of SMC methods has proven to be effective even in the presence of input saturation [15], [16]. Another method employs a virtual system with the difference between the theoretical input and saturated control input, and designs a sliding surface that relies on tracking error and virtual state to handle saturation nonlinearity [17]. However, in aerospace/aerial PSIS, the inertia cannot be evaluated exactly, and the upper bound of system uncertainty and external disturbance is difficult to obtain, which limits its applications. Theoretically, it is necessary to select a sufficiently large switching gain in SMC to suppress them, which in turn leads to high energy consumption and causes severe system chattering [18].

Consequently, adaptive sliding mode control (ASMC) is presented to eliminate bound dependency and attenuate chattering, which has been applied and explored in the aerospace/aerial field. An ASMC methodology was proposed in [19] for tethered satellite deployment with input saturation. An ASMC for attitude stabilization of a spacecraft system with actuator saturation was proposed [20], and no prior knowledge of the inertia moment is required. A new adaptation laws is designed to assign a minimum admissible value to the switching gain [21]. In [22], an adaptive fast terminal SMC law was presented for a rigid spacecraft to provide finite-time convergence, strong robustness, and fault-tolerant control. However, previous studies have mostly focused on control methods that are effective in the presence of input saturation, or consider input saturation as a nonlinear disturbance, and research on methods that can make systems out of saturation in a short time, little research on how to use the drive capacity of the actuator more fully to improve the system tracking speed when saturation is unavoidable. In addition, previously reported adaptive laws lack strategies on adaptive parameters that accumulate when the actuator is saturated repeatedly. When saturation occurs and disappears, the adaptive parameters do not automatically reduce to the initials, leading to unexpected continuous chattering.

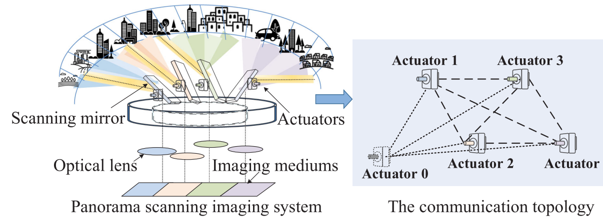

Fig. 1. PSIS with multiple actuators.

The actuator saturation state corresponds to the maximum drive capacity. Inspired by the abovementioned analysis and discussion, this study aims to investigate a novel ASMC method for multiple actuators in an aerospace/aerial PSIS subject to input saturation and model uncertainties with effective imaging commands. The main contributions of this study are as follows:

1) An ASMC scheme with a saturation coefficient (ASMC-SC) is proposed. By designing a nonlinear sliding surface, whose parameter is adjusted according to the SC, the actuator drive capability is more fully utilized, and the tracking performance is improved. Meanwhile, the adaptive parameters with SC for the ASMC are proposed, and undesired accumulations of adaptive parameters are avoided when the actuators are saturated frequently, which suppresses system chattering.
2) The uniformly ultimate boundedness (UUB) of the proposed ASMC-SC is provided using Lyapunov stability arguments and the ultimately bounded tracking errors are guaranteed.
3) The proposed method is implemented on scanning mirror bases with saturation limits and model uncertainties. Simulations and experiments demonstrate that the convergence and tracking performances of the proposed ASMC-SC are improved compared to the traditional ASMC method.

The rest of this article is organized as follows. System description is presented in Section II. The strategy design and stability proof of the proposed adaptive sliding mode cooperative control with a SC is discussed in Section III. Numerical simulations and experiments were performed to verify the effectiveness of the proposed approach, which are presented in Section IV. Section V concludes this article.

II. PROBLEM FORMULATION

A. System Description

A PSIS with multiple actuators is shown in Fig. 1. The PSIS is composed of one fictitious actuator (labeled as actuator 0) and N actual actuators (labeled as actuator 1, . . ., N), which tracks the motion of the fictitious actuator and achieves continuous scan imaging. To achieve a wider coverage under a limited FOV, multiple scanning mirrors were controlled for cooperative imaging. To ensure that images acquired via the scanners can be stitched together to create a high-definition panoramic image, complete synchronization of multiple scanners is required. The control objective of the PSIS is that the position and velocity of all actual actuators can be stabilized to converge to the expected position and velocity of the fictitious actuator with high speed.

The dynamics of the fictitious actuator in PSIS is described as follows:

$$\begin{cases} \dot{x}_0 = v_0 \\ \dot{v}_0 = f(x_0, v_0) + c_0 u_0 \end{cases} \tag{1}$$

where $x_0, v_0 \in \mathbb{R}^n$ are the position and velocity state variables of the fictitious actuator, respectively; $f(x_0, v_0)$ are the items related to the characteristics of the control plant, n denotes the motion dimension of the actuator, and $u_0 \in \mathbb{R}^n$ is the control input.

The dynamics of the ith ($i = 1, \ldots, N$) actual actuators are given by

$$\begin{cases} \dot{x}_i = v_i \\ \dot{v}_i = f(x_i, v_i) + c_i u_i + d_i \end{cases} \tag{2}$$

where $x_i, v_i \in \mathbb{R}^n$ are the position and velocity state variables, and $u_i \in \mathbb{R}^n$ is the control input. d_i is the equivalent disturbance, including external disturbance and model uncertainties. PSIS is driven by a voice coil motor, and there are mechanical frames and isolators on its outside to isolate wind resistance, carrier vibration, and other external disturbances. Generally, the disturbance subjected to actuators of PSIS is relatively small. Without loss of generality, $N = 4$ in this article.

Assumption 1 It is assumed that that there exists an upper bound of d_i in (2), satisfying

$$\|d_i\| \le \bar{d}, i = 1, \ldots, N \tag{3}$$

Assumption 2 According to the Lipschitz condition, there exists nonnegative constants ζ_1 and ζ_2, such that

$$\begin{aligned} &||f(x, v) - f(x', v')|| \le \zeta_1 ||x - x'|| + \zeta_2 ||v - v'|| \\ &\quad \forall x, x', v, v' \in \mathbb{R}^n. \end{aligned} \tag{4}$$

To simplify the mathematical representation of multi-actuator coimaging and stability analysis, graph theory is introduced to describe the communication topology and the corresponding information interaction among actuators of scanning mirrors.

Let $G = (V, E, A)$ be a graph of N nodes, which represents the communication topology between the N actual actuators. $V = \{\nu_1, \ldots, \nu_N\}$ and $E \subseteq V \times V$ are the node set and edge set of G, respectively. $A = [a_{ij}] \in \mathbb{R}^{N\times N}$ represents an adjacency matrix and $L_G = [l_{ij}] \in \mathbb{R}^{N\times N}$ is the Laplace matrix, where $l_{ii} = \sum_{i\neq j} a_{ij}$, $l_{ij} = -a_{ij} (i \neq j)$.

The interactive information between the fictitious actuator and actual actuators is represented by a diagonal matrix $B_G = \text{diag}\{b_1, \ldots, b_N\}$, and $b_i \ge 0, i = 1, \ldots N$. Then, an augmented graph $\bar{G}$ is applied to denote the communication topology between the fictitious actuator and all actual actuators. Assume that for PSIS, at least one actual actuator in the augmented graph $\bar{G}$ obtains information from the fictitious actuator, and each actuator obtains the relative motion information from its neighboring actuators only. Then, the communication network between actuators is connected.

B. Cooperative Scan and Stability

Define the position and velocity tracking error as $\tilde{x}_i = x_i - x_0$, $\tilde{v}_i = v_i - v_0$, $i = 1, \ldots, N$, the ideal control objective of the PSIS can be expressed as follows:

$$\begin{aligned} &\lim_{t\to\infty} \tilde{x}_i = 0_n \\ &\lim_{t\to\infty} \tilde{v}_i = 0_n, i = 1, \ldots, N. \end{aligned} \tag{5}$$

The aerospace/aerial imaging circumstances of the PSIS are relatively complex, unknown dynamics, complex internal, and external disturbances, noise, etc., making it difficult to realize an ideal cooperative scan. Consequently, the control objective for the PSIS is to design a multiactuator controller so that the position and velocity tracking errors $\tilde{x}_i$ and $\tilde{v}_i$, $i = 1, \ldots N$ can converge to a small neighborhood of zero. To ensure that the PSIS can maintain good cooperative performance under disturbances, the UUB concept, describing the robust stability of uncertain systems, was introduced [23].

Definition 1 (UUB): For the PSIS with N actual actuators, the control objective is there exist compact sets $\Omega^{\tilde{x}}, \Omega^{\tilde{v}} \subset R^{N\times n}$ containing the origin, so that for $\forall \tilde{x}(t_0) \in \Omega^{\tilde{x}}$ and $\forall \tilde{v}(t_0) \in \Omega^{\tilde{v}}$, there exist bounds $B^{\tilde{x}}$, $B^{\tilde{v}}$ and time $T(B^{\tilde{x}}, B^{\tilde{v}}, \tilde{x}(t_0), \tilde{v}(t_0))$, such that $\|\tilde{x}(t)\| \le B^{\tilde{x}}$ and $\|\tilde{v}(t)\| \le B^{\tilde{v}}$, for $\forall t \ge t_0 + T(B^{\tilde{x}}, B^{\tilde{v}}, \tilde{x}(t_0), \tilde{v}(t_0))$, where $\tilde{x} = [\tilde{x}_1^T, \ldots, \tilde{x}_N^T]^T$, $\tilde{v} = [\tilde{v}_1^T, \ldots, \tilde{v}_N^T]^T$.

Define the control errors of the PSIS as

$$\begin{aligned} e_{xi} &= \sum_{j=1}^{N} l_{ij}(x_j - x_i) + b_i(x_i - x_0) \\ e_{vi} &= \sum_{j=1}^{N} l_{ij}(v_j - v_i) + b_i(v_i - v_0), i = 1, \ldots, N. \end{aligned} \tag{6}$$

Let $e_x = [e_{x1}^T, \ldots, e_{xN}^T]^T$, $e_v = [e_{v1}^T, \ldots, e_{vN}^T]^T$, the control error is given by

$$\begin{aligned} e_x &= (L_G + B_G) \otimes I_n \cdot \tilde{x} \\ e_v &= (L_G + B_G) \otimes I_n \cdot \tilde{v} \end{aligned} \tag{7}$$

where $I_n = \text{diag}\{1, \ldots, 1\} \in \mathbb{R}^{n\times n}$, and $\otimes$ denotes the Kronecker product.

Consequently, the dynamics of the control error system of the PSIS are written as

$$\begin{aligned} \dot{e}_x &= e_v \\ \dot{e}_v &= (L_G + B_G) \otimes I_n \cdot (F - F_0 + D + U - U_0) \end{aligned} \tag{8}$$

where $F = [f(x_1, v_1)^T, \ldots, f(x_N, v_N)^T]^T$, $F_0 = 1_N \otimes f(x_0, v_0)$, $D = [d_1^T, \ldots, d_N^T]^T$, $U = [c_1 u_1^T, \ldots, c_N u_N^T]^T$, $U_0 = 1_N \otimes c_0 u_0$, $1_N = [1, \ldots, 1]^T \in \mathbb{R}^N$.

Consequently, it can be deduced that the problem of the cooperative scan of the PSIS, as shown in (1) and (2)

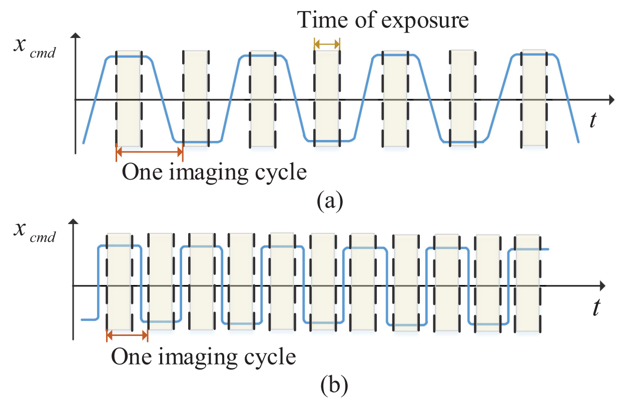

Fig. 2. Actuator motion commands. (a) Periodic trapezoidal wave command. (b) Periodic rectangular wave command.

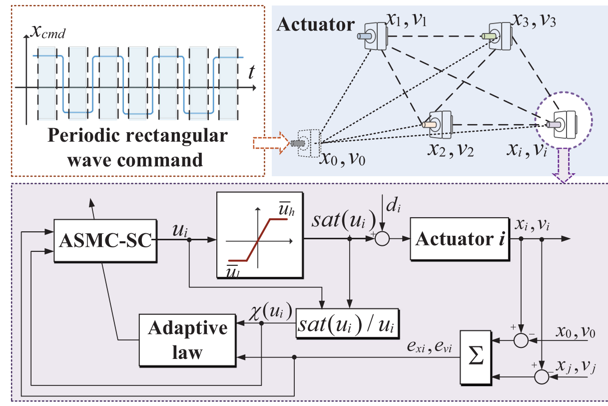

Fig. 3. Block diagram of the proposed ASMC-SC.

is transformed into a stability problem of the control error system, as shown in (8).

C. Multiactuators Control Under High-Efficiency Control Command With Input Saturation

To meet the urgent requirements of imaging efficiency for advanced PSIS, the control command has been changed from a periodic trapezoidal wave command, as shown in Fig. 2(a) to periodic rectangular wave command preprocessed without infinite derivatives as Fig. 2(b), under which limited actuator drive capability leads to control input saturation, which is an inevitable nonsmooth nonlinear characteristic of the practical system. The occurrence of input saturation subsequently deteriorates the system performance and even destabilizes the control system.

Considering the input saturation, the control inputs u_0 and u_i in (1) and (2) are replaced by $\mathrm{sat}(u_0)$ and $\mathrm{sat}(u_i)$, respectively, where $\mathrm{sat}(u_0) = [\mathrm{sat}(u_{01}), \ldots, \mathrm{sat}(u_{0n})]^T$ when $n > 1$ is the actual control input, which is the same as $\mathrm{sat}(u_i)$. $\mathrm{sat}(u)$ denotes the nonlinear saturation function with input u, and its mathematical description is

$$\mathrm{sat}(u) = \begin{cases} \bar{u}_h, & u > \bar{u}_h \\ u, & \bar{u}_l \le u \le \bar{u}_h \\ \bar{u}_l, & u < \bar{u}_l \end{cases} \tag{9}$$

where $\bar{u}_h > 0$ and $\bar{u}_l < 0$ are the known upper and lower bounds of the control input, respectively.

To treat the control constraint more conveniently, the saturation function in (9) is expressed as

$$\mathrm{sat}(u) = \chi(u)u \tag{10}$$

$\chi(u)$ is the SC, which can be written as

$$\chi(u) = \begin{cases} \bar{u}_h/u, & u > \bar{u}_h \\ 1, & \bar{u}_l \le u \le \bar{u}_h. \\ \bar{u}_l/u, & u < \bar{u}_l \end{cases} \tag{11}$$

where $\chi(u) \in (0, 1]$ and when $\chi(u) = 1$, the actuator works normally; when $\chi(u) \to 0$, the actuator is in deep saturation and most of the control variable cannot be output; when $0 < \chi(u) < 1$, the actuator works but its drive capacity has been completely exhausted and cannot fully execute the controller commands.

Thus, (8) is transformed as

$$\begin{aligned} \dot{e}_x &= e_v \\ \dot{e}_v &= (L_G + B_G) \otimes I_n \cdot (F - F_0 + D + \chi(U)U - \chi(U_0)U_0) \end{aligned} \tag{12}$$

where $\chi(U_0) = \mathrm{diag}\{\chi(U_{01}), \ldots, \chi(U_{0N})\}$ when $N > 1$, the same as $\chi(U)$.

III. STRATEGY DESIGN OF MULTIACTUATORS CONTROL FOR THE PSIS

Generally, the design procedure of the proposed ASMC-SC is divided into two parts:

1) Design of a sliding surface s with a SC. Once multiactuators are saturated, the PSIS can maximize the maximum drive capacity of the actuators, such that the dynamic response of PSIS is faster, and the reaching time of multiactuators to the sliding surface $s = 0$ is shorter.
2) An ASMC scheme with adaptive parameters designed by introducing a SC is developed, and undesired accumulations of adaptive parameters are avoided when the actuators are saturated frequently under a highly efficient periodic rectangular wave command.

The two parts above are developed in this section, and the stability is discussed in three cases according to whether the actuators in PSIS are saturated. A block diagram of the proposed control scheme is illustrated in Fig. 3.

A. Sliding Surface Design With SC

To meet the urgent requirements of imaging efficiency for advanced PSIS, a periodic rectangular wave command is designed, which inevitably brings actuator saturation owing to the limited actuator drive capacity. However, owing to the advantage of rapidity for SMC, the characteristics of a traditional linear sliding surface make the system state out of input saturation quickly, and the system state converges to command slowly because the actuators are unable to use their driving capacity fully, which is in conflict with the requirement of efficient panorama scanning imaging.

To make full use of the actuator's drive capability in the presence of input saturation, a nonlinear sliding surface is designed as

$$s = M_a e_x + e_v. \tag{13}$$

where $s = [s_1^T, \ldots, s_N^T]^T$, $s_i = \mu_{ai} e_{xi} + e_{vi}$, $M_a = \text{diag}\{\mu_{a1}, \ldots, \mu_{aN}\} \otimes I_n$, $\mu_{ai} = \frac{\mu_i}{T(\chi(u_i))}$, $\bar{\mu}_{al} \leq \| \mu_{ai} \| \leq \bar{\mu}_{ah}$, and $\bar{\mu}_{al}, \bar{\mu}_{ah} > 0$, $i = 1, \ldots, N$.

A nonlinear function $T(\chi(u_i))$ is introduced in the design of the sliding surface and is expressed as

$$T(\chi(u_i)) = \tanh(g_T/(1 - \chi(u_i))) \tag{14}$$

where $0 < g_T < 1$, $\tanh(x) = \frac{\sinh x}{\cosh x} = \frac{e^x - e^{-x}}{e^x + e^{-x}}$. Because $\chi(u_i) \in (0, 1]$, $T(\cdot) \in (\bar{T}, 1)$ and $\bar{T} > \tanh(g_T) > 0$.

$T(\chi(u_i))$ is a continuous differential function, which ensures that the proposed nonlinear sliding surface changes smoothly when actuator switches between saturated and unsaturated states. When the actuator is saturated, the nonlinear function $T(\chi(u_i))$ decreases promptly as the degree of saturation increases, the parameter of the sliding surface is adjusted according to the SC and increases speedily. The deeper the control input enters saturation, the greater the sliding mode parameter μ_{ai}, more fully the actuator drive capability is utilized, the more rapidly the system can escape from the saturation state and the faster the position response converges to the expectation, the need for efficient scanning imaging can be better realized.

If the sliding condition $s = 0_{n\times N}$ can be satisfied with the control error system, as shown in (8), the control objective of PSIS is given by (5).

B. ASMC Scheme With SC

Adaptive control is introduced into the control strategy to suppress actuator chattering and reduce the system energy consumption. Thus, the control protocol in this study is given by

$$U = (L_G + B_G)^{-1} \otimes I_n \cdot (-s + B_G \otimes I_n \cdot U_0 + w(s)) \tag{15}$$

where $w(s) = [w_1^T(s), \ldots, w_N^T(s)]^T$.

During the specific implementation, the control variable for the ith actuator is calculated using

$$u_i = c_i^{-1} (l_{ii} + b_i)^{-1} \left(-\sum_{j\neq i} l_{ij} u_j + c_0 b_i u_0 - s_i + w_i(s_i) \right). \tag{16}$$

$w(s)$ is expressed as

$$w_i(s_i) = -\hat{\rho}_i \text{sgn}(s_i) \tag{17}$$

where $\hat{\rho}_i$ is an adaptive control parameter designed as

$$\hat{\rho}_i = \hat{k}_{0i} + \hat{k}_{xi}\|e_{xi}\| + \hat{k}_{vi}\|e_{vi}\|, i = 1, \ldots, N. \tag{18}$$

In the slide stage, the actuator control error moves on the sliding surface, and the system has robustness to model uncertainties and compound disturbances.

Existing adaptive sliding mode methods consider the influence of saturation on system stability in the design of a control strategy for a single actuator; however, the accumulation of adaptive parameters leads to additional control input jitter when the actuator enters the saturation state repeatedly. When the system is in the slide stage and control input saturation occurs, the system state will leave the slide stage quickly, and its position and velocity errors will increase significantly. At this time, if the adaptive parameters are modified with control error, the system will diverge easily.

In fact, the symbolic function part plays an important role in the slide stage, when the SC should work, while losing efficacy after the system leaves the slide stage due to control input saturation. Consequently, the SC is introduced into the update law of the adaptive parameters as follows:

$$\dot{\hat{k}}_{0i} = \begin{cases} p_{0i}(\|s_i\| - \lambda_{0i}\hat{k}_{0i}), & \chi(u_i) = 1 \\ 0, & \chi(u_i) < 1 \end{cases} \tag{19}$$

$$\dot{\hat{k}}_{xi} = \begin{cases} p_{xi}(\|s_i\|\|e_{xi}\| - \lambda_{xi}\hat{k}_{xi}), & \chi(u_i) = 1 \\ 0, & \chi(u_i) < 1 \end{cases} \tag{20}$$

$$\dot{\hat{k}}_{vi} = \begin{cases} p_{vi}(\|s_i\|\|e_{vi}\| - \lambda_{vi}\hat{k}_{vi}), & \chi(u_i) = 1 \\ 0, & \chi(u_i) < 1 \end{cases} \tag{21}$$

where $p_{0i} > 0$, $p_{xi} > 0$, $p_{vi} > 0$, $\lambda_{0i} > 0$, $\lambda_{xi} > 0$, $\lambda_{vi} > 0$, $i = 1, \ldots, N$.

C. Stability Analysis of the Proposal

THEOREM 1 Suppose Assumptions 1 and 2 are valid, then the ultimate boundedness of multiactuators in the PSIS with input saturation is achieved under the proposed ASMC-SC as

PROOF: Consider the following Lyapunov function candidate

$$V = \frac{1}{2}\left[s^T s + \sum_{i=1}^{N} \frac{1}{p_{0i}} \tilde{k}_{0i}^2 + \sum_{i=1}^{N} \frac{1}{p_{xi}} \tilde{k}_{xi}^2 + \sum_{i=1}^{N} \frac{1}{p_{vi}} \tilde{k}_{vi}^2 \right], \tag{22}$$

where $\tilde{k}_{0i} = \bar{k}_0 - \hat{k}_{0i}$, $\tilde{k}_{xi} = \bar{k}_x - \hat{k}_{xi}$, $\tilde{k}_{vi} = \bar{k}_v - \hat{k}_{vi}$ are the parameter estimation errors. $\bar{k}_0$, $\bar{k}_x$, and $\bar{k}_v$ are the upper bounds of $\hat{k}_{0i}$, $\hat{k}_{xi}$ and $\hat{k}_{vi}$, $i = 1, \ldots, N$, respectively.

Its derivative is

$$\begin{aligned} \dot{V} = {} & s^T(M_a e_v + (L_G + B_G) \otimes I_n \cdot (F - F_0 + D)) \\ & + \chi(U) s^T(w(s) - s) + (\chi(U) \\ & - \chi(U_0)) s^T (L_G + B_G) U_0 \\ & - \sum_{i=1}^{N} \frac{1}{p_{0i}} \tilde{k}_{0i} \dot{\hat{k}}_{0i} - \sum_{i=1}^{N} \frac{1}{p_{xi}} \tilde{k}_{xi} \dot{\hat{k}}_{xi} - \sum_{i=1}^{N} \frac{1}{p_{vi}} \tilde{k}_{vi} \dot{\hat{k}}_{vi}. \end{aligned} \tag{23}$$

Setting the control input bound of actual actuators slightly less than that of the input bound of the fictitious actuator, $\chi(U) < \chi(U_0)$ can be deduced; then

$$\dot{V} \le s^T(M_a e_v + (L_G + B_G) \otimes I_n \cdot (F - F_0 + D)) + \chi(U)s^T(w(s) - s) - \sum_{i=1}^{N} \frac{1}{p_{0i}} \tilde{k}_{0i}\dot{\hat{k}}_{0i} - \sum_{i=1}^{N} \frac{1}{p_{xi}} \tilde{k}_{xi}\dot{\hat{k}}_{xi} - \sum_{i=1}^{N} \frac{1}{p_{vi}} \tilde{k}_{vi}\dot{\hat{k}}_{vi}. \tag{24}$$

According to Assumption 2, it can be deduced that

$$\begin{aligned}\|F - F_0\| &= \|[\|f(x_1, v_1) - f(x_0, v_0)\|, \\ &\quad \ldots, \|f(x_N, v_N) - f(x_0, v_0)\|]^T\| \\ &\le \|[\zeta_1\|\tilde{x}_1\| + \zeta_2\|\tilde{v}_1\|, \ldots, \zeta_1\|\tilde{x}_N\| + \zeta_2\|\tilde{v}_N\|]^T\| \\ &\le \zeta_1\|\tilde{x}\| + \zeta_1\|\tilde{v}\|.\end{aligned} \tag{25}$$

From (7), this yields

$$\begin{aligned}\|(L_G + B_G) \otimes I_n \cdot (F - F_0)\| &\le \|(L_G + B_G)\|(\zeta_1\|\tilde{x}\| + \zeta_2\|\tilde{v}\|) \\ &\le \zeta_1\|e_x\| + \zeta_2\|e_v\|.\end{aligned} \tag{26}$$

Then, with Assumption 1, we obtain

$$\begin{aligned}&M_a e_v + (L_G + B_G) \otimes I_n(F - F_0 + D) \\ &\le \zeta_1\|e_x\| + (\bar{\mu}_{ah} + \zeta_2)\|e_v\| + \|(L_G + B_G)\|\sqrt{N}\bar{d}.\end{aligned} \tag{27}$$

Let $\Psi_1 = \zeta_1\|e_x\| + (\bar{\mu}_{ah} + \zeta_2)\|e_v\| + \|(L_G + B_G)\|\sqrt{N}\bar{d}$, then

$$\dot{V} \le \Psi_1\|s\| + \chi(U)s^T(w(s) - s) - \sum_{i=1}^{N} \frac{1}{p_{0i}} \tilde{k}_{0i}\dot{\hat{k}}_{0i} - \sum_{i=1}^{N} \frac{1}{p_{xi}} \tilde{k}_{xi}\dot{\hat{k}}_{xi} - \sum_{i=1}^{N} \frac{1}{p_{vi}} \tilde{k}_{vi}\dot{\hat{k}}_{vi}. \tag{28}$$

Case 1: all of the actuators work properly

If $\chi(u_i) = 1$, $i = 1, \ldots, N$, it can be deduced that:

$$\begin{aligned}\dot{V} &\le \Psi_1\|s\| - \sum_{i=1}^{N}(\hat{k}_{0i} + \hat{k}_{xi}\|e_{xi}\| + \hat{k}_{vi}\|e_{vi}\|)\|s_i\| - \|s\|^2 \\ &\quad - \sum_{i=1}^{N}\tilde{k}_{0i}(\|s_i\| - \lambda_{0i}\hat{k}_{0i}) - \sum_{i=1}^{N}\tilde{k}_{xi}(\|s_i\|\|e_{xi}\| - \lambda_{xi}\hat{k}_{xi}) \\ &\quad - \sum_{i=1}^{N}\tilde{k}_{vi}(\|s_i\|\|e_{vi}\| - \lambda_{vi}\hat{k}_{vi}) \\ &= \Psi_1\|s\| - \|s\|^2 - \sum_{i=1}^{N}(\bar{k}_0 + \bar{k}_x\|e_{xi}\| + \bar{k}_v\|e_{vi}\|)\|s_i\| \\ &\quad + \sum_{i=1}^{N}\lambda_{0i}\tilde{k}_{0i}\hat{k}_{0i} + \sum_{i=1}^{N}\lambda_{xi}\tilde{k}_{xi}\hat{k}_{xi} + \sum_{i=1}^{N}\lambda_{vi}\tilde{k}_{vi}\hat{k}_{vi}\end{aligned} \tag{29}$$

Because $\tilde{k}_{0i}\hat{k}_{0i} = (\bar{k}_{0i} - \hat{k}_{0i})\hat{k}_{0i}$, the maximum is $\bar{k}_0^2/4$ when $\hat{k}_{0i} = \bar{k}_0/2$. Similarly, the maxima of $\tilde{k}_{xi}\hat{k}_{xi}$ and $\tilde{k}_{vi}\hat{k}_{vi}$ are $\bar{k}_x^2/4$ and $\bar{k}_v^2/4$, respectively. Set $\bar{\lambda}_0$, $\bar{\lambda}_x$, $\bar{\lambda}_v$ as the upper bounds of $\lambda_{0i}, \lambda_{xi}, \lambda_{vi}$, $i = 1, \ldots, N$, respectively. Then

$$\begin{aligned}\dot{V} &\le \Psi_1\|s\| - \|s\|^2 - \sum_{i=1}^{N}(\bar{k}_0 + \bar{k}_x\|e_{xi}\| + \bar{k}_v\|e_{vi}\|)\|s_i\| \\ &\quad + \frac{\bar{\lambda}_0}{4}\sum_{i=1}^{N}\bar{k}_0^2 + \frac{\bar{\lambda}_x}{4}\sum_{i=1}^{N}\bar{k}_x^2 + \frac{\bar{\lambda}_v}{4}\sum_{i=1}^{N}\bar{k}_v^2.\end{aligned} \tag{30}$$

Set $\eta_{a1} = N(\bar{\lambda}_0\bar{k}_0^2 + \bar{\lambda}_x\bar{k}_x^2 + \bar{\lambda}_v\bar{k}_v^2)/4$. Then $\exists\Psi_2 = \inf(\bar{k}_0 + \bar{k}_x\|e_{xi}\| + \bar{k}_v\|e_{vi}\|)$ and $\Psi_3 = \inf(\bar{\mu}_{al}\|e_{xi}\| + \|e_{vi}\|)$ for $i = 1, \ldots, N$, hence

$$\begin{aligned}\dot{V} &\le -(\Psi_2 + \Psi_3 - \Psi_1)\|s\| + \eta_{a1} \\ &\le -\Psi_a\|s\| + \eta_{a1}\end{aligned} \tag{31}$$

where $\Psi_a = \Psi_2 + \Psi_3 - \Psi_1$.

Case 2: all of the actuators are saturated

If $\chi(u_i) < 1$, $i = 1, \ldots, N$, from the point of view of physical implementation, the SC cannot indefinitely approach zero as the practical control input is derived from a finite system response. Mathematically, the density property of real numbers states that between any two real numbers, there is another real number [24]; hence, the following Assumption 3 holds

ASSUMPTION 3 There exists a constant $\bar{\chi}$ that $0 < \bar{\chi} < \min\{\chi(u_1), \ldots, \chi(u_N)\} \le 1$.

Then, it can be deduced that

$$\begin{aligned}\dot{V} &\le \Psi_1\|s\| - \bar{\chi}\sum_{i=1}^{N}(\hat{k}_{0i} + \hat{k}_{xi}\|e_{xi}\| + \hat{k}_{vi}\|e_{vi}\|)\|s_i\| - \bar{\chi}\|s\|^2 \\ &\le -(\Psi_2 + \Psi_3 - \Psi_1)\|s\| \\ &\quad + \bar{\chi}\sum_{i=1}^{N}(\bar{k}_0 + \bar{k}_x\|e_{xi}\| + \bar{k}_v\|e_{vi}\|)\|s_i\|.\end{aligned} \tag{32}$$

According to the Cauchy–Schwarz inequality, $\sum_{i=1}^{N}\bar{k}_0\|s_i\| \le N^{1/2}\bar{k}_0\|s\|$, $\sum_{i=1}^{N}\bar{k}_x\|e_{xi}\|\|s_i\| \le \bar{k}_x\|e_x\|\|s\|$, $\sum_{i=1}^{N}\bar{k}_v\|e_{vi}\|\|s_i\| \le \bar{k}_v\|e_v\|\|s\|$. Hence

$$\dot{V} \le -\Psi_a\|s\| + \eta_{a_2}. \tag{33}$$

where $\eta_{a_2} = \bar{\chi}(N^{1/2}\bar{k}_0 + \bar{k}_x\|e_x\| + \bar{k}_v\|e_v\|)\|s\|$.

Case 3: part of the actuators are saturated

If $\chi(u_i) < 1$ for some actuators, $\chi(u_i) = 1$ for the other actuators. Similar to the analysis in Case 1 and 2, it can be derived that

$$\dot{V} \le -\Psi_a\|s\| + \eta_{a_3}. \tag{34}$$

where the value of η_{a_3} is between η_{a_1} and η_{a_2}.

In this article, it is assumed that disturbances other than input saturation have been precompensated in the feedforward loop, $\bar{d}$ is small. For the actuators in PSIS, ζ_1, ζ_2 are usually small constants. Therefore, $\Psi_a \ge 0$ can be guaranteed by setting the adaptive parameters appropriately. Combining the above three cases yields the following inequality for any $\chi(u_i)$, $i = 1, \ldots, N$ by setting $\eta_a = \max\{\eta_{a1}, \eta_{a2}\}$.

$$\begin{aligned}\dot{V} &\leq -\Psi_a\|s\| + \eta_a \\ &\leq -(1-\delta_a)\Psi_a\|s\|, \forall\|s\| \geq \frac{\eta_a}{\delta_a\Psi_a}\end{aligned} \tag{35}$$

where $0 < \delta_a < 1$. The sliding surface s reaches a boundary layer given as follows:

$$\Omega_{a1} = \left\{\|s\| \leq \frac{\eta_a}{\delta_a\Psi_a}\right\}. \tag{36}$$

Inside the boundary, as shown in (36), according to (13), $\dot{e}_x = -M_a e_x + s$. Then, the derivative of $V_{ex} = \frac{1}{2}e_x^T e_x$ satisfies

$$\begin{aligned}\dot{V}_{ex} &\leq -M_a e_x^T e_x + e_x^T s \\ &\leq -\bar{\mu}_{al}\|e_x\|^2 + \frac{\eta_a}{\delta_a\Psi_a}\|e_x\| \\ &\leq -(1-\delta_{e_x})\bar{\mu}_{al}\|e_x\|^2, \forall\|e_x\| \geq \frac{1}{\delta_{e_x}\bar{\mu}_{al}}\frac{\eta_a}{\delta_a\Psi_a}\end{aligned} \tag{37}$$

where $0 < \delta_{e_x} < 1$.

Equation (37) indicates that e_x will reach the set $\Omega_{e_x} = \{\|e_x\| \leq \frac{\eta_a}{\delta_{e_x}\bar{\mu}_{al}\delta_a\Psi_a}\}$, and e_x is ultimately bounded. Owing to the fact as (13) and (36), e_v also reaches a boundary layer and is ultimately bounded.

REMARK 1 From (35) and (37), we note that the control error system in (8) is uniformly ultimately bounded. Then, the ultimate boundedness goal of the cooperative motion of the PSIS is achieved. Thus, the trajectory of the control error system in (8) will reach the sliding surface, and the state errors e_x and e_v will be ultimately bounded at an exponential rate. This concludes the proof.

IV. SIMULATIONS AND EXPERIMENTS

A. Simulations

To illustrate the effectiveness of the proposed ASMC-SC, the tracking performance of the PSIS composed of a fictitious actuator and four actual actuators is simulated in this section. The topology of PSIS is shown in Fig. 1. In general, for actuators in the PSIS, $f(x_i, v_i) = -\frac{B}{J}v_i, c_i = \frac{1}{J}, i = 0, 1, \ldots, N$, where J and B are the inertia and damping, respectively. The inertia and damping of the fictitious actuator are $0.00217\,\text{kg}\cdot\text{m}^2$ and $0.15\,\text{Ns/m}$, respectively. Considering model uncertainties, the inertia and damping of the actuators were chosen as $[0.0021, 0.0023, 0.00213, 0.0022]\,\text{kg}\cdot\text{m}^2$, and $[0.155, 0.139, 0.142, 0.16]\,\text{Ns/m}$, respectively. The saturation limits are $\bar{u}_h = 8.5$ and $\bar{u}_l = -7.5$. According to a preexperiment result by disturbance evaluation on a scanning mirror base, the maximum value of the disturbance is set as $0.2\,\text{N}\cdot\text{m}$.

The initial conditions of the adaptive factors $p_{0i}(0)$, $p_{xi}(0)$, and $p_{vi}(0)$ are $0.0002, 0.005, 0.1$, $\hat{k}_{0i}(0), \hat{k}_{xi}(0), \hat{k}_{vi}(0)$ are $0.1, 0.01, 0.01$, λ_{0i}, λ_{xi}, and λ_{yi} are $0.28, 0.1, 0.1$, respectively. $g_T = 1/30$ and $\mu_i = 6.25$ for $i = 1, \ldots N$. The sampling time was 1 ms and the position sensor noise was $0.0007°$. A flowchart of the control algorithm for actuator i is shown in Fig. 4.

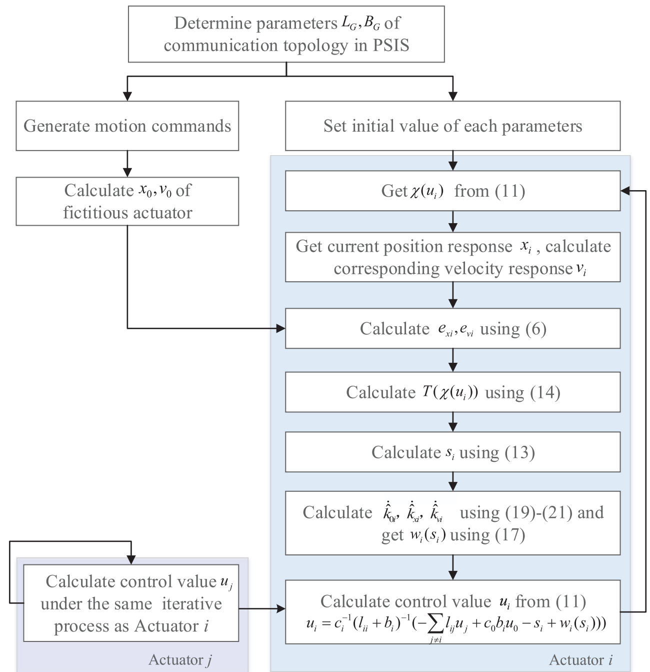

Fig. 4. Flowchart of the proposed algorithm for actuator i.

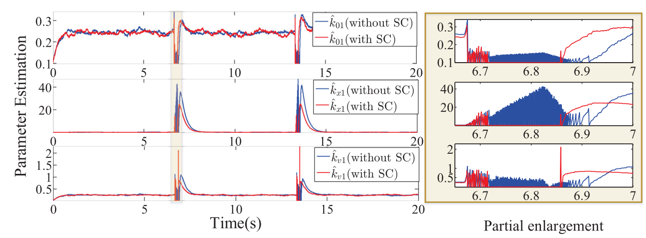

Fig. 5. Convergence of adaptive parameters value with sliding surface with/without SC and its partial enlargement.

Case 1: The control performance comparison using the proposed sliding surface and traditional sliding surface

The convergence of the adaptive parameters is simulated in Fig. 5 to demonstrate the advantage of the sliding surface in (13), as proposed in Section III, compared with the sliding surface without the SC.

Periodic rectangular wave commands frequently make actuators in and out of the saturation state, which leads to the control error e_x and e_v to vary greatly over a relatively short time. Thus, motion chattering can be easily introduced. It is shown that the proposed sliding surface achieves good performance in adaptive parameter convergence, with less parameter chattering in spite of input saturation during the command switch.

Case 2: The control performance comparison between the proposed ASMC-SC and traditional ASMC

The control performance under the proposed ASMC-SC and traditional ASMC without a SC are compared. The position trajectories are shown in Fig. 6. The initial position of the actual actuators was chosen randomly in the

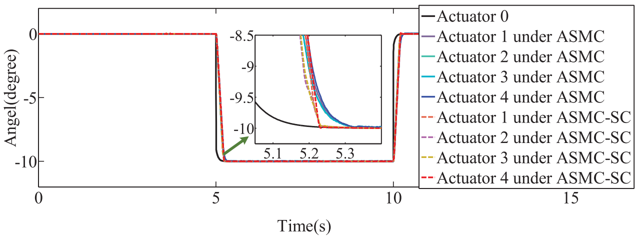

Fig. 6. Convergence performance of multiactuators under ASMC-SC and ASMC.

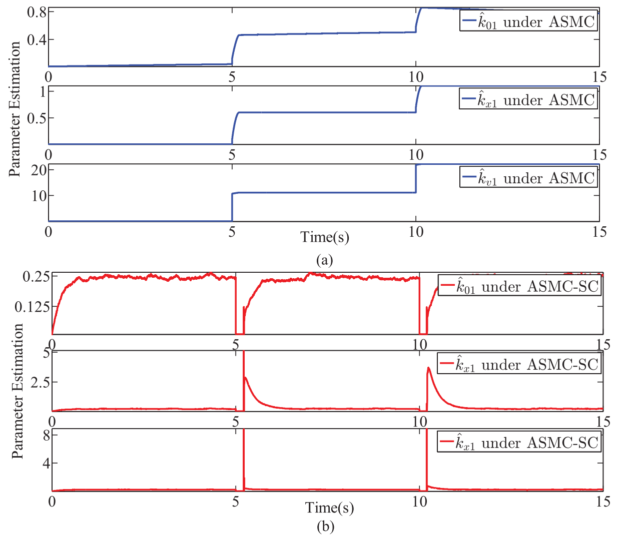

Fig. 7. Adaptive parameters under ASMC and ASMC-SC. (a) Adaptive parameters of Actuator 1 under ASMC, (b) Adaptive parameters of Actuator 1 under ASMC-SC.

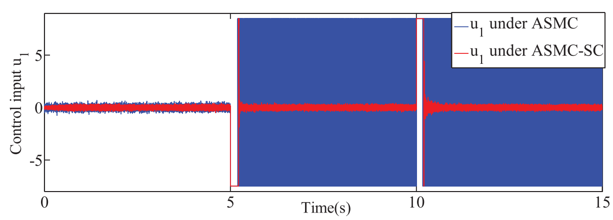

Fig. 8. Actuator control input comparison under ASMC-SC and ASMC.

range $[-2^\circ, 2^\circ]$, and the initial velocity values were chosen randomly in the range $[-3, 3]^\circ/\mathrm{s}$.

Because the SC is considered in the design of the sliding surface and adaptive parameters, the proposed method could improve the convergence performance by utilizing the actuator drive capability more adequately when input saturation occurs.

Fig. 7 shows the corresponding trajectory of estimated adaptive parameters for Actuator 1 under the periodic rectangular wave command. It is clear that the parameters $\hat{k}_{01}$, $\hat{k}_{x1}$, $\hat{k}_{v1}$ converges under the proposed ASMC-SC, while the parameters accumulated significantly under ASMC because the tracking error become large when actuator is saturated for each command switch.

A control input comparison between the ASMC-SC and ASMC is shown in Fig. 8. Obviously, adaptive parameter accumulations of ASMC due to input saturation lead to

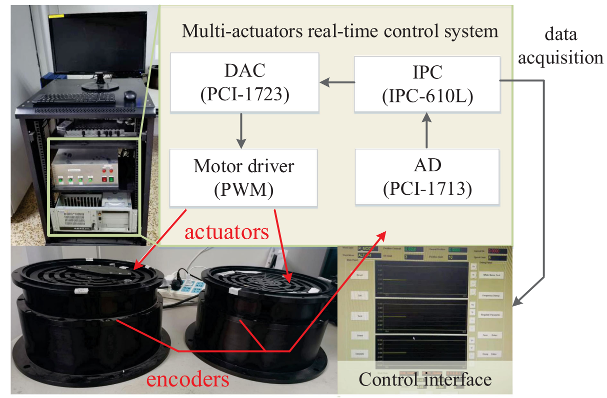

Fig. 9. Experimental setup of scanning mirror bases.

undesired chattering, which affects the actual motion performance of the PSIS.

B. Experiments

The proposed method was verified experimentally. Owing to the restriction of experimental conditions and equipment, practical experiments were implemented on two scanning mirror bases with two brushless DC(BLDC) rotary motors ($N = 2$), where scanning mirrors fix on for scanning a fixed imaging area. The required differential calculation was performed using a nonlinear tracking differentiator in [25]. The control algorithms were programmed in the C language into a Linux-based real-time system with a GCC environment. This real-time operational system was installed on an industrial personal computer (Advantech IPC-610 L). The control value was output to the motor driver through a digital-to-analog (D/A) converter card (Advantech PCI-1723). The analog signal of the encoder was converted to a digital signal through an AD card (Advantech PCI-1713). The motor driver was a pulsewidth modulation (PWM)-driven current controller. The position responses were measured using optical-electricity encoders with a resolution of 0.00007°. The sampling time is 1 ms, which is much higher than the bandwidth of the encoder to ensure that the control error for each control point is obtained quickly enough, and the corresponding control is calculated. The experimental setup is illustrated graphically in Fig. 9.

The inertia and damping of the fictitious actuator were set as $0.0025\mathrm{kg}\cdot\mathrm{m}^2$ and $0.015\mathrm{Ns/m}$, respectively. The inertia of the two scanning mirror bases is $0.0025\mathrm{kg}\cdot\mathrm{m}^2$ and $0.00272\mathrm{kg}\cdot\mathrm{m}^2$, and the damping is $0.024\mathrm{Ns/m}$ and $0.0176\mathrm{Ns/m}$, respectively. The saturation limit is $\bar{u}_h = \bar{u}_l = 4$. The initial conditions of the adaptive factors $p_{0i}(0)$, $p_{xi}(0)$, and $p_{vi}(0)$ are 0.01, 0.08, 0.07, $\hat{k}_{0i}(0)$, $\hat{k}_{xi}(0)$, $\hat{k}_{vi}(0)$ are 0.01, 0.001, 0.001, λ_{0i}, λ_{xi}, and λ_{yi} are 0.15, 0.05, 0.05, respectively. $g_T = 10/7$ and $\mu_1 = \mu_2 = 2.1$.

Fig. 10 shows that the proposed ASMC-SC can achieve better tracking performance compared with ASMC without SC, and therefore guarantee higher imaging efficiency. Figs. 11 and 12 demonstrate the corresponding adaptive parameters and control inputs under ASMC-SC and ASMC

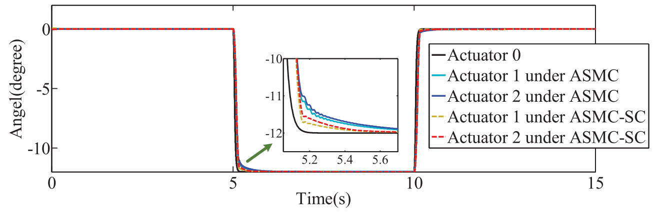

Fig. 10. Experimental tracking performance of scanning mirror bases under ASMC-SC and ASMC.

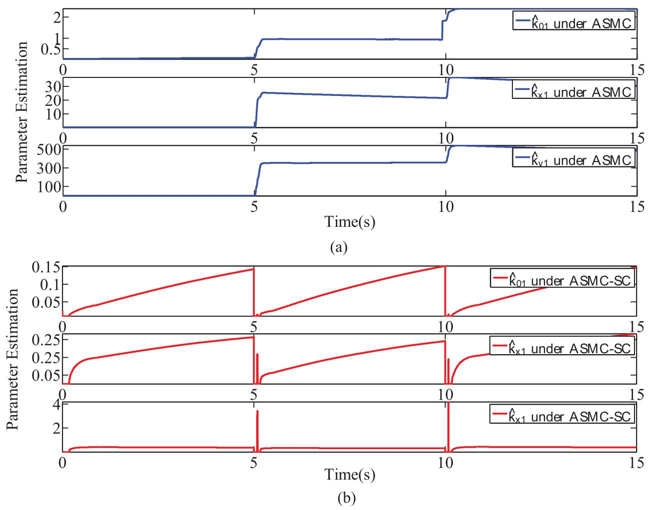

Fig. 11. The experimental adaptive parameters of scanning mirror bases under ASMC and ASMC-SC. (a) Adaptive parameters of Actuator 1 under ASMC. (b) Adaptive parameters of Actuator 1 under ASMC-SC.

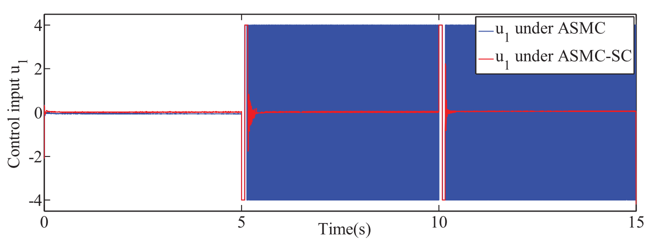

Fig. 12. Experimental control inputs of scanning mirror bases under ASMC-SC and ASMC.

without SC. It can be concluded that the proposed ASMC-SC exhibits stronger robustness to input saturation.

V. CONCLUSION

In this article, we proposed a novel ASMC-SC control algorithm by introducing a SC into the design procedure of the sliding surface and adaptive parameters. Theoretical analyses of UUB are proved by the Lyapunov function method. Simulations and experimental results demonstrate that the ASMC-SC scheme has better convergence and motion performances compared with ASMC without a SC. In the future, the proposal will be extended to multiactuators suffering from more complex disturbances. An optimal control allocation scheme and minimum SMC gains will also be considered to further minimize the control energy and suppress chattering, respectively.

REFERENCES

[1] F. Xiao, Z. Ding, and M. Ke
Imaging algorithm for multi-channel scan synthetic aperture radar with channel error estimation and compensation
J. Eng., vol. 2019, no. 20, pp. 6688–6691, Jul. 2019.

[2] W. Lyu, S. Dai, Y. Dong, Y. Shen, X. Song, and T. Wang
Attitude motion compensation for imager on Fengyun-4 geostationary meteorological satellite
Acta Astronautica, vol. 138, pp. 290–294, Sep. 2017.

[3] Y. Sun, J. Zeng, Y. Li, P. Rao, and T. Hu
Compensation method for the image motion of a rotary-scan space camera
Opt. Quantum Electron., vol. 52, pp. 502-1–502-15, Nov. 2020.

[4] M. Ramachandran, M. Agarwal, and D. Daniel
Efficient onboard image motion compensation for orbital inclination and eccentricity of geostationary weather satellites
Proc. Inst. Mech. Eng. Part G, J. Aerosp. Eng., vol. 234, pp. 1311–1325, 2020.

[5] D. Tian, Y. Wang, F. Wang, and Y. Zhang
Bilateral control-based compensation for rotation in imaging in scan imaging systems
Opt. Eng., vol. 54, Dec. 2015, Art. no. 124104.

[6] Q. Chen, S. Xie, M. Sun, and X He
Adaptive nonsingular fixed-time attitude stabilization of uncertain spacecraft
IEEE Trans. Aerosp. Electron. Syst., vol. 54, no. 6, pp. 2937–2950, Dec. 2018.

[7] T. Hayakawa, T. Watanabe, T. Senoo, and M. Ishikawa
Gain-compensated sinusoidal scanning of a galvanometer mirror in proportional-integral-differential control using the pre-emphasis technique for motion-blur compensation
Appl. Opt., vol. 55, no. 21, pp. 5640–5646, Jul. 2016.

[8] D. Tian, Y. Wang, Z. Wang, F. Wang, and H. Gao
Long integral time continuous panorama scanning imaging based on bilateral control with image motion compensation
Remote Sens., vol. 11, no. 16, Aug. 2019, Art. no. 1924.

[9] M. Chen, B. Ren, Q. Wu, and J. CS
Anti-disturbance control of hypersonic flight vehicles with input saturation using disturbance observer
Sci. China Inf. Sci., vol. 58, Jul. 2015, Art. no. 70202.

[10] Y. Wang, Y. Tuo, S. X. Yang, M. Biglarbegian, and M. Fu
Reliability-based robust dynamic positioning for a turret-moored floating production storage and offloading vessel with unknown time-varying disturbances and input saturation
ISA Trans., vol. 78, pp 66–79, 2018.

[11] J. Du, X. Hu, M. Krsti, and Y. Sun
Robust dynamic positioning of ships with disturbances under input saturation
Automatica, vol. 73, pp. 207–214, Nov. 2016.

[12] Y. Huang and Y. Jia
Adaptive finite-time 6-DOF tracking control for spacecraft fly-around with input saturation and state constraints
IEEE Trans. Aerosp. Electron. Syst., vol. 55, no, 6, pp. 3259–3272, Dec. 2019.

[13] J. Monteiro, F. Lizarralde, and H. Liu
Optimal control allocation of quadrotor UAVs subject to actuator constraints
In *Proc. Amer. Control Conf.*, 2016, pp. 500–505.

[14] A. Vahidi-Moghaddam *et al.*
Terminal sliding mode control with non-symmetric input saturation for vibration suppression of electrostatically actuate d nanob eams in the presence of Casimir force
Appl. Math. Modelling, vol. 60, pp. 416–434, Jul. 2018.

[15] X. Shi, Y. Zhang, D. Zhou, and Z. Zhou
Global fixed-time attitude tracking control for the rigid spacecraft with actuator saturation and faults
Acta Astronautica, vol. 155, pp. 325–333, Feb. 2019.

[16] B. Jiang, Q. Hu, and M. Friswell
Fixed-time attitude control for rigid spacecraft with actuator saturation and faults
IEEE Trans. Control Syst. Technol., vol. 24, no. 5, pp. 1892–1898, Sep. 2016.

[17] Y. Zheng and H. Cui
Disturbance observer-based robust guidance for Mars atmospheric entry with input saturation
Chin. J. Aeronaut., vol. 28, no, 3, pp. 845–852, Apr. 2015.

[18] H. Chen, S. Song, and Z. Zhu
Robust finite-time attitude tracking control of rigid spacecraft under actuator saturation
Int. J. Control Automat. Syst., vol. 16, no. 1, pp. 1–15, Mar. 2018.

[19] Z. Ma and G. Sun
Adaptive sliding mode control of tethered satellite deployment with input limitation
Acta Astronautica, vol. 127, pp. 67–75, Nov. 2016.

[20] Z. Zhu, Y. Xia, and M. Fu
Adaptive sliding mode control for attitude stabilization with actuator saturation
IEEE Trans. Ind. Electron., vol. 58, no. 10, pp. 4898–4907, Oct. 2011.

[21] J. Zhu and K. Khayati
New algorithms of adaptive switching gain for sliding mode control: Part II - Real case
In *Int. Conf. Control Decis. Inf. Technol.*, 2014, pp. 447–452.

[22] K. Lu, Y. Xia, C. Yu, and H. Liu
Finite-time tracking control of rigid spacecraft under actuator saturations and faults
IEEE Trans. Automat. Sci. Eng., vol. 13, no. 1, pp. 368–381, Jan. 2016.

[23] H. Khalil
Nonlinear System, 3rd ed. Upper Saddle River, NJ, USA: Prentice-Hall, 2002.

[24] Q. Shen, D. Wang, S. Zhu,, and K. Poh
Finite-time fault-tolerant attitude stabilization for spacecraft with actuator saturation
IEEE Trans. Aerosp. Electron. Syst., vol. 51, no. 3, pp. 2390–2405, Mar. 2015.

[25] D. Tian, H. Shen, and M. Dai
Improving the rapidity of nonlinear tracking differentiator via feedforward
IEEE Trans. Industy Electron., vol. 61, no. 7, pp. 3736–3743, Jul. 2014.

Yutang Wang (Member, IEEE) received the B.E. degree in automation and the M.S. degree in control science and engineering in 2009 and 2012, respectively, from the Beijing Institute of Technology. She received the Ph.D. degree in optical engineering from the University of Chinese Academy of Sciences, China, in 2019.

Since 2012, she has been with the Key Laboratory of Airborne Optical Imaging and Measurement, Changchun Institute of Optics, Fine Mechanics and Physics, Chinese Academy of Sciences, China. Her current research interests include optical imaging and motion control.

Dapeng Tian (Senior Member, IEEE) received the B.E. degree in aircraft design from Beijing Institute of Technology, Beijing, China, in 2007. He received the Ph.D. degree in control science from Beihang University, Beijing, China, in 2012.

He was then directly recommended to study at Beihang University, Beijing, China. From 2009 to 2011, he was a co-Researcher with the Advanced Research Center, Keio University, Yokohama, Japan. Since 2012, he has been with the Key Laboratory of Airborne Optical Imaging and Measurement, Changchun Institute of Optics, Fine Mechanics and Physics, Chinese Academy of Sciences, Changchun, China, where he is currently a Full Professor. His current research interests include motion control theory and engineering, optical imaging, and bilateral control.

Rui Xu received the Ph.D. degree in control theory and control engineering from Jilin University, Changchun, China, in 2019.

From 2018 to 2019, he was an exchange Ph.D. Student in Michigan State University, East Lansing, MI, USA. Since 2020, he has been with the Key Laboratory of Airborne Optical Imaging and Measurement, Changchun Institute of Optics, Fine Mechanics and Physics, Chinese Academy of Sciences, Changchun, China. His current research interests include micronano drive control, motion control theory, and optical imaging.